



**HAL**  
open science

# Demonstration of a ceria membrane solar reactor promoted by dual perovskite coatings for continuous and isothermal redox splitting of CO<sub>2</sub> and H<sub>2</sub>O

Anita Haeussler, Stéphane Abanades, Julien Jouannaux, Anne Julbe

## ► To cite this version:

Anita Haeussler, Stéphane Abanades, Julien Jouannaux, Anne Julbe. Demonstration of a ceria membrane solar reactor promoted by dual perovskite coatings for continuous and isothermal redox splitting of CO<sub>2</sub> and H<sub>2</sub>O. *Journal of Membrane Science*, 2021, 634, pp.119387. 10.1016/j.memsci.2021.119387 . hal-03365953

**HAL Id: hal-03365953**

**<https://hal.science/hal-03365953>**

Submitted on 5 Oct 2021

**HAL** is a multi-disciplinary open access archive for the deposit and dissemination of scientific research documents, whether they are published or not. The documents may come from teaching and research institutions in France or abroad, or from public or private research centers.

L'archive ouverte pluridisciplinaire **HAL**, est destinée au dépôt et à la diffusion de documents scientifiques de niveau recherche, publiés ou non, émanant des établissements d'enseignement et de recherche français ou étrangers, des laboratoires publics ou privés.

# Demonstration of a ceria membrane solar reactor promoted by dual perovskite coatings for continuous and isothermal redox splitting of CO<sub>2</sub> and H<sub>2</sub>O

Anita HAEUSSLER<sup>1</sup>, Stéphane ABANADES<sup>1\*</sup>, Julien JOUANNAUX<sup>2</sup>, Anne JULBE<sup>2</sup>

<sup>1</sup> Processes, Materials and Solar Energy Laboratory, CNRS-PROMES, 7 Rue du Four Solaire, 66120 Font-Romeu, France

<sup>2</sup> Institut Européen des Membranes, IEM, UMR-5635, ENSCM, CNRS, Univ Montpellier, Place Eugène Bataillon, 34095 Montpellier cedex 5, France

\* Corresponding author: Tel +33 (0)4 68 30 77 30

E-mail address: stephane.abanades@promes.cnrs.fr

## Abstract:

The direct one-step CO<sub>2</sub> and H<sub>2</sub>O splitting using an oxygen-transport membrane (OTM) reactor was investigated as a potentially ideal way to generate renewable fuels from concentrated solar energy. The solar-driven thermolysis of CO<sub>2</sub> (or H<sub>2</sub>O) was promoted by *in-situ* oxygen removal across nonstoichiometric ceria-based membranes. A new solar membrane reactor integrating a tubular densified membrane made of either pure ceria or perovskite-coated ceria was designed and operated under high-flux concentrated solar radiation. A continuous flow of inert gas on the permeate side was used to create the required oxygen partial pressure gradient (driving force) and ensure continuous oxygen permeation via oxygen ion diffusion across the densified ceria membrane. The continuous OTM solar operation at high temperature was demonstrated through testing under various operating conditions. The CO and O<sub>2</sub> production rates were sharply enhanced by increasing the operating temperature (up to 1550°C). The increase of CO<sub>2</sub> concentration or oxidant gas flow rate also enhanced the process performance. Unprecedented fuel production rates (>0.07 μmol s<sup>-1</sup> cm<sup>-2</sup> at 1550°C) were achieved with a pure CO<sub>2</sub> stream on the feed side and flowing Ar on the sweep side of the reactive ceria membrane. An original composite membrane integrating two different perovskite coatings on each side of the ceria membrane, with a sandwich-like structure, was designed and tested under concentrated sunlight. Thin layers of La<sub>0.5</sub>Sr<sub>0.5</sub>Mn<sub>0.9</sub>Mg<sub>0.1</sub>O<sub>3</sub> on the inner side and Ca<sub>0.5</sub>Sr<sub>0.5</sub>MnO<sub>3</sub> on the outer side were added to enhance oxygen ion transfer. With such a membrane configuration, a

remarkable production of CO ( $>0.13 \mu\text{mol s}^{-1} \text{cm}^{-2}$ ) and oxygen (with CO:O<sub>2</sub> ratio of 2) was obtained simultaneously, respectively on the inner and outer sides of the OTM. These results outperform the production rates achieved with the uncoated ceria membranes, and demonstrate the benefits of using composite membranes composed of a densified core material coated with (or sandwiched in between) redox active perovskite materials.

**Keywords:** solar fuel, solar membrane reactor, perovskite-coated ceria, oxygen transport, thermochemical redox splitting

## 1. Introduction

Thermochemical H<sub>2</sub>O and CO<sub>2</sub> splitting processes are a promising solution to free the worldwide energy production from fossil fuels and reach a carbon neutral economy by producing sustainable fuels. Indeed, two-step thermochemical cycles produce CO and H<sub>2</sub> from abundant and low-cost feedstocks (H<sub>2</sub>O and CO<sub>2</sub>) and solar heat as sole inputs, while a reactive metal oxide is regenerated [1,2]. Thus, such processes can be considered as carbon neutral provided that the required energy input is renewable such as concentrated solar heat. They further offer high theoretical solar-to-fuel energy conversion efficiency without requiring any electrical power input, as opposed to the electrochemical pathway. The produced hydrogen can be directly used (*e.g.* in fuel cells) whereas syngas (a mixture of CO and H<sub>2</sub>) can be converted into valuable products such as liquid hydrocarbons *via* Fischer-Tropsch synthesis, or methanol. This pathway represents one of the emerging and most promising processes for solar thermochemical fuel production and for the recycling and valorization of anthropogenic greenhouse gas emissions [3–6]. CO<sub>2</sub> is converted into a valuable product (CO) that can be further processed to liquid fuels when combined with H<sub>2</sub>. Furthermore, the oxygen produced during the reduction step can be stored and used for other applications (*e.g.* oxy-combustion).

As main issues, two-step thermochemical cycles require large temperature swing and produce solar fuels sequentially in separate steps with temperature and/or pressure change. Temperature swing induces heat losses due to multiple cooling/heating stages, which negatively impact the solar-to-fuel conversion extent. Furthermore, it can also damage the reactor internal ceramic components and the reactive material due to thermal stress. Thus, a process able to split directly CO<sub>2</sub> (or H<sub>2</sub>O) by performing both steps (reduction and oxidation) simultaneously appears as highly attractive since solar fuels could be produced continuously and isothermally. A membrane reactor with an oxygen-selective membrane is a relevant option for reaching this goal [7–10]. In such a process, a reactive mixed ionic-electronic conducting (MIEC) membrane acts as an oxygen exchanger between both reaction zones and oxygen transfer medium to separate the produced O<sub>2</sub> and CO (or H<sub>2</sub>) streams, as shown in Figure 1. On the reduction side (sweep side), maintained at low oxygen partial pressure, the membrane

releases oxygen, thus creating oxygen vacancies, corresponding to reaction (1). According to Fick's law, the oxygen ions captured from CO<sub>2</sub> (or H<sub>2</sub>O) on the oxidation side tend to migrate through the membrane toward the reduction side to re-equilibrate the oxygen vacancies created at the membrane surface. On the oxidation side (feed side), oxygen vacancies are refilled during CO<sub>2</sub> (or H<sub>2</sub>O) splitting reaction, thereby leading to CO (or H<sub>2</sub>) production, corresponding to reaction (2). These reactions occurring simultaneously produce solar fuels continuously. As O<sub>2</sub> and CO (H<sub>2</sub>) are separated by the membrane, recombination cannot occur.

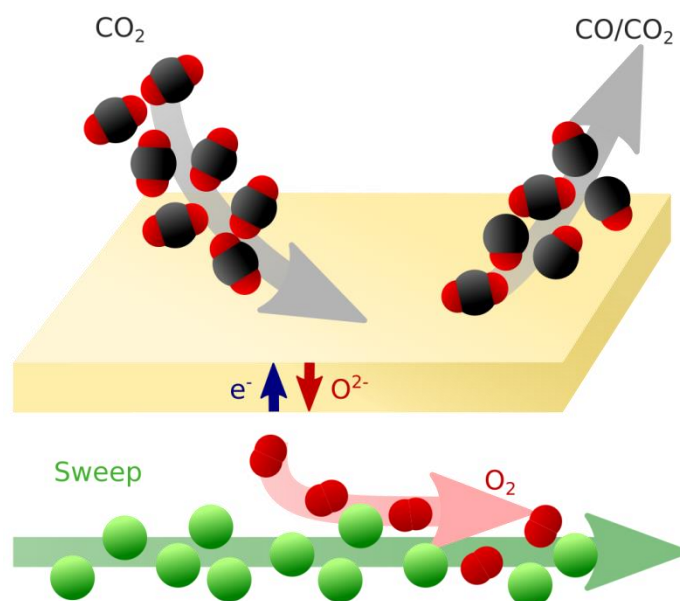
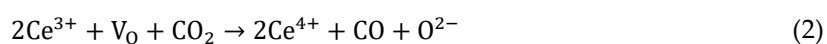
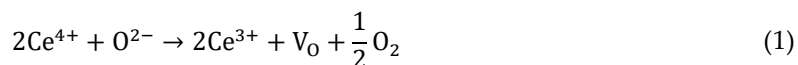


Figure 1: Schematic representation of the CO<sub>2</sub> dissociation process with a mixed ionic-electronic conducting membrane: the reduction side is maintained at low oxygen partial pressure thanks to inert gas flow (sweep) to favor a continuous transfer of oxygen ions and electrons across the membrane

In order to perform such a solar-driven combined-step process, the reactive membrane should satisfy the following conditions:

- offer mixed ionic-electronic conduction and high selectivity for O<sub>2</sub> transport;
- be dense enough to separate the products via oxygen ion diffusion through the membrane thickness (without any molecular diffusion of gas species through interconnected pores or defects);
- provide high oxygen ion diffusivity within the temperature range used for CO<sub>2</sub> (or H<sub>2</sub>O) splitting;

- maintain its crystallographic structure over a large range of experimental conditions, especially at high temperature (above 1400°C).

The available surface area of the reactive membrane is also a key parameter (to be maximized) for CO<sub>2</sub> dissociation [7,11]. Dense ceramic membrane technologies were considered for several applications, including air separation [12,13], air separation combined with methane partial oxidation [14], methane reforming [15] or nitrogen monoxide and nitrous oxide dissociation [16]. A membrane reactor using a perovskite-disc membrane to perform air separation was developed [17]. The reactive membrane (La<sub>0.4</sub>Ba<sub>0.6</sub>Fe<sub>0.8</sub>Zn<sub>0.2</sub>O<sub>3</sub>) was coupled with a commercial methane reforming catalyst. A gas mixture He/CH<sub>4</sub> was supplied to the reduction side of the membrane, resulting in methane partial oxidation to CO without any NO<sub>x</sub> production. On the membrane opposite side, synthetic air was continuously injected, providing a pure oxygen flux of 0.9 cm<sup>3</sup>/cm<sup>2</sup>/min at 950°C through a 0.5 mm thick membrane.

Perovskite-based membranes were also studied to produce continuously H<sub>2</sub> and syngas (H<sub>2</sub>/CO mixture) by water splitting coupled with partial oxidation of methane, and the highest H<sub>2</sub> production rate was 3.4 μmol/cm<sup>2</sup>/s with BaCo<sub>x</sub>Fe<sub>y</sub>Zr<sub>1-x-y</sub>O<sub>3</sub> membrane [18]. Other membranes such as SrCo<sub>0.4</sub>Fe<sub>0.5</sub>Zr<sub>0.1</sub>O<sub>3</sub> [19], SrCo<sub>0.8</sub>Fe<sub>0.2</sub>O<sub>3</sub> [20], La<sub>0.6</sub>Sr<sub>0.4</sub>Co<sub>0.2</sub>Fe<sub>0.8</sub>O<sub>3</sub> [15] or La<sub>1-x</sub>Sr<sub>x</sub>Fe<sub>1-y</sub>M<sub>y</sub>O<sub>3</sub> (M=Ni, Co, Cr, Cu, Mn) [21,22] were investigated as well for CO<sub>2</sub> reforming to produce syngas. Jin et al. [19] developed a membrane reactor using a dense BaCo<sub>x</sub>Fe<sub>y</sub>Zr<sub>1-x-y</sub>O<sub>3</sub> perovskite disk membrane coated with Nd/Al<sub>2</sub>O<sub>3</sub> and Pd/SrCo<sub>0.4</sub>Fe<sub>0.5</sub>Zr<sub>0.1</sub>O<sub>3</sub> catalysts. On the oxidation side, a CO<sub>2</sub>/He mixture was injected, resulting in CO production, while a CH<sub>4</sub>/Ar gas mixture was injected on the reduction side, resulting in syngas production. The experiment was run in the temperature range 850-950°C and the oxygen flux through the membrane reached 1.36 mL/cm<sup>2</sup>/min at 950°C.

Fluorite-based membrane processes were investigated for the direct dissociation of CO<sub>2</sub> and H<sub>2</sub>O. In 1993, Itoh et al. [23] proposed for the first time this concept to thermally decompose CO<sub>2</sub> using a reactive membrane. An yttria-stabilized zirconia membrane in the temperature range of 1311-1509°C led to CO<sub>2</sub> conversion extent of 0.6%. Nigara et al. [24] highlighted the ability of ZrO<sub>2</sub>-CeO<sub>2</sub>-CaO membrane to dissociate H<sub>2</sub>O at high temperature. Hydrogen was also produced by direct water splitting at high temperature using a reactive ZrO<sub>2</sub>-TiO<sub>2</sub>-Y<sub>2</sub>O<sub>3</sub> membrane. A sufficiently low value of oxygen partial pressure is required in order to ensure a mixed ionic-electronic conduction in such fluorite material, while a high gradient of oxygen partial pressure is required in order to ensure a sufficient driving force for charge transport through the membrane [25].

More recently, Tou et al. [7,26,27] developed a ceria reactive membrane to produce CO from CO<sub>2</sub> dissociation. The reactor was composed of an inert alumina tube heated by artificial concentrated solar flux. The reactive membrane was placed inside the alumina tube and was indirectly heated. The membrane inner side was fed with CO<sub>2</sub>, leading to CO production, while Ar swept the membrane

outer side to remove the oxygen released by the membrane. A maximum CO production of  $0.024 \mu\text{mol}/\text{cm}^2/\text{s}$  was achieved under  $3 \cdot 10^{-6}$  bar  $p_{\text{O}_2}$  at  $1600^\circ\text{C}$ .

This study aims to demonstrate the feasibility of isothermal and continuous  $\text{CO}_2$  (or  $\text{H}_2\text{O}$ ) splitting using ion-conducting redox active membranes. The single-step thermolysis process is based on the utilization of a mixed ionic-electronic conducting ceria membrane at the high temperatures provided by concentrated solar energy. The oxygen vacancies created on the reduction side at low oxygen partial pressure are filled by promoting  $\text{CO}_2$  or  $\text{H}_2\text{O}$  splitting on the oxidation side. Ceria ( $\text{CeO}_2$ ) was selected as a relevant membrane material with rapid reaction kinetics, high oxygen diffusion rates and exchange properties, and excellent resistance to high temperatures. Tubular dead-end membranes were used for *in-situ* separation of the reaction products via oxygen transfer through the membrane, from the oxidation side to the reduction side. A parametric study of the solar membrane reactor was performed to investigate the relevant operating parameters impacting the thermochemical system performance. Furthermore, substantial efforts were also devoted to the development of a composite membrane configuration with appropriate dual perovskite coatings on each side to achieve noticeable performance improvements. The analysis of experimental performance with reactive uncoated and perovskite-coated ceria membranes was carried out to compare their fuel production capacity in the solar membrane reactor. This study demonstrated for the first time the application of such membranes for the single-step  $\text{CO}_2$  (or  $\text{H}_2\text{O}$ ) splitting using a solar-driven membrane reactor under real concentrated solar radiation. The obtained results represent an important step forward in the development of novel solar-driven membrane reactors for production of separate streams of  $\text{O}_2$  and  $\text{CO}$  (or  $\text{H}_2$ ) using oxygen-conducting redox materials.

## 2. Experimental methods

### 2.1. Membrane synthesis and shaping

The pristine tubular ceria membranes were provided by ALSYS-CTI. These membranes were prepared from commercial ceria powders (Marion Technologies), by slip-casting of optimized slurries, drying and sintering ( $1600^\circ\text{C}$  during 5 h). Three reactive densified membranes (1.8 mm thick) were used to produce solar fuels. These membranes include an uncoated ceria membrane (Figure 2.a) and two perovskite-coated ceria membranes (Figure 2.b and c), abbreviated as UC, PCC1 and PCC2, respectively. The outer side of the PCC membranes was coated with  $\text{Ca}_{0.5}\text{Sr}_{0.5}\text{MnO}_3$  (CSM) perovskite while the inner side was coated with  $\text{La}_{0.5}\text{Sr}_{0.5}\text{Mn}_{0.9}\text{Mg}_{0.1}\text{O}_3$  (LSMMg). The UC and PCC2 membranes were 150 mm long whereas the PCC1 membrane was only 135 mm long; the other dimensions are given in Figure 2.d. The perovskite coatings were deposited by slip-casting (inside) and dip-coating (outside), using suitable optimized slurries. For both LSMMg and CSM perovskite formulations, the powder (synthesis with P2 Pechini method [28]) was dispersed in water (45 wt %) using a

polymethacrylate dispersing agent (DARVAN C-N®) and polyvinyl alcohol (Rhodoviol, 2 wt%) as a binder/plasticizer. A SpeedMixer® (DAC 150.1 FVZ-K) was used to obtain fluid, uniform, stable and smooth slurries, suitable for casting. For the inside LSMMg coating, the membrane was filled with the slurry, up to the membrane flange during 90 s. Then, the membrane was turned over to let the excess slurry flowing freely. For applying the external coating, the ceria tube was immersed in the CSM slurry during 90 s and then removed at a rate of 0.5 cm/min. In between the two deposition steps, the membranes were dried for 30 min at 100°C and weighted. The mass uptake after the LSMMg coating was estimated at 0.5% while it was ~0.2% for the CSM coating due to the different procedure. The membranes went through a multi-step thermal treatment with a final sintering in air at 1500°C for 8 h (2°C/min ramp). After this final thermal treatment, the coatings exhibited surface defects that may be due to local variations of the porosity, roughness or other types of defects of the ceria membrane support (such as cracks or molding irregularities) and that alter the uniformity of the perovskite coatings thickness. The prepared membranes used in this study are shown in Figure 2. The coating on PCC2 membrane was thinner than PCC1 and some zones of the ceria support appeared uncovered by the perovskite layer (especially for PCC2). This presumably indicates that the effect of the perovskite coating will be enhanced in the case of PCC1. Although the thickness of the coatings is not perfectly uniform, the CSM layer typically corresponds to the size of one grain (10-25 µm thick) while the LSMMg layer (0.5-3 µm thick) is composed of several smaller grains. The membrane tubes are closed at one end (dead-end tubes or finger type) and fitted with a flange (collar shape) for tight fixation. The reactive surface area of membranes was considered as the area exposed to solar irradiation in the cavity (including the capped tube end), corresponding to 26 cm<sup>2</sup> for both UC and PCC2 membranes and 22 cm<sup>2</sup> for the shorter PCC1 membrane.

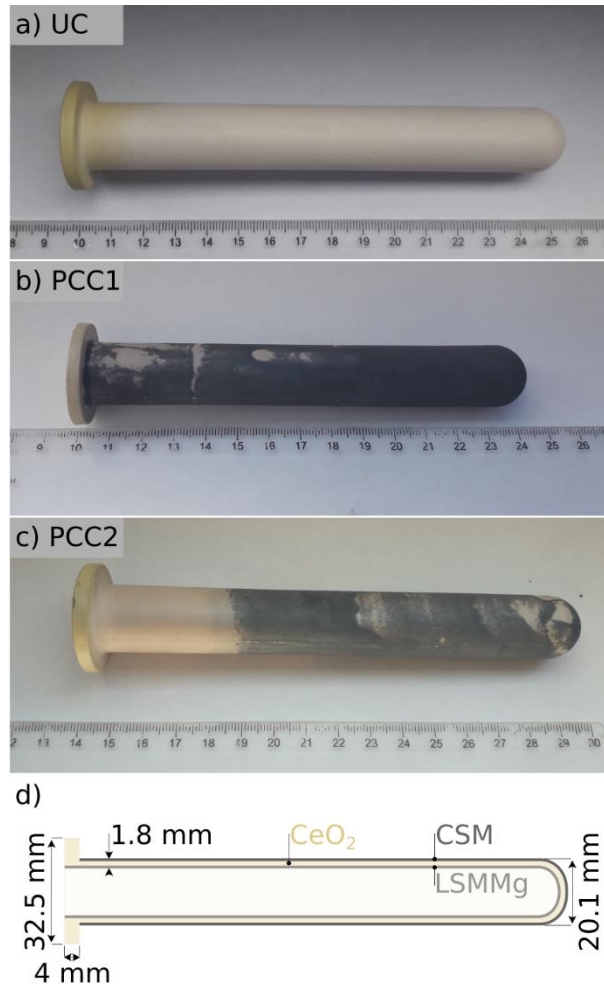


Figure 2: Reactive membranes used in the continuous thermochemical splitting process, a) pure uncoated ceria (UC) tube, b) and c) perovskite-coated ceria (PCC1 and PCC2) tubes, d) scheme of the dead-end membrane tube and dimensions

## 2.2. Solar membrane reactor

Isothermal experiments using ceria-based membranes to continuously produce solar fuels with *in-situ* extraction/pumping of the produced oxygen across the membrane, were performed in a vertical-axis medium-size solar facility of PROMES-CNRS laboratory (SUNFUEL reactor). The solar reactor was placed at the focus of a parabolic dish irradiated by a sun-tracking heliostat. The solar reactor was designed to produce continuously solar fuels thanks to a reactive membrane able to separate the two redox reaction steps and the gas products (Figure 3). The cavity was composed of an alumina cylinder (50 mm inner diameter and 80 mm height) with a lateral opening to let the membrane pass horizontally through it and it was closed by an alumina top-cover with 19 mm diameter aperture. The cavity configuration permits both to maximize the absorbed concentrated solar radiation and to minimize the solar re-radiation loss from the cavity to the surrounding environment. The effective active area of the membrane being heated by the absorbed solar energy corresponds to the zone inserted within the reactor cavity (~50 mm length). A hermetical transparent Pyrex window on top of the reactor allows the solar radiation to reach the cavity receiver/reaction chamber. A water-cooling

system was used to cool the stainless-steel reactor shell and flanges in order to avoid sealing damages due to high temperatures. The reactive membrane was installed in the reactor thanks to a support fixed on the reactor side, resulting in  $\sim 26 \text{ cm}^2$  of the membrane surface being exposed to high-temperature solar heat inside the solar-cavity receiver. Seals on the membrane flange were used to prevent any gas transfer between the inner and outer sides of the membrane as well as any leak between the reactor and the outside. The reactive membrane was used as an oxygen transferring medium: its outside surface releases oxygen (reduction reaction) while its inner surface is re-oxidized with  $\text{CO}_2$  (or  $\text{H}_2\text{O}$ ). A  $\text{CO}_2/\text{Ar}$  gas mixture (or steam) was injected inside the membrane tube via an alumina pipe (6x4 mm) fixed to the membrane support. The extremity of the pipe reached the heated zone (extremity of the membrane tube), so that the oxidative gas swept the whole membrane length. In case water was used as an oxidant, liquid water was injected in a stainless steel capillary inserted inside the alumina pipe, and then vaporized at the capillary exit (tip placed just before the cavity zone) and transported by Ar carrier gas flowing inside the alumina pipe.

At the exit of the tubular membrane (inner side), the outlet gas was analyzed by an online gas analyzer (Emerson Xstream) equipped with IR ( $\text{CO}/\text{CO}_2$ , 0-40% for CO, 0-100% for  $\text{CO}_2$ ) and thermal conductivity detector ( $\text{H}_2$ , 0-50%). Regarding the reduction side of the membrane, an Ar flow (99.9999% purity,  $[\text{O}_2] < 2 \text{ ppm}$ ) was injected from the reactor bottom toward the Pyrex window via two stainless steel pipes in order to sweep the window area and then entered the cavity to flow in the downward direction. The  $\text{O}_2$  released by the membrane was thus continuously evacuated from the cavity by the Ar carrier gas. The Ar/ $\text{O}_2$  mixture was continuously analyzed by a trace  $\text{O}_2$  electrochemical analyzer (Systech, range from 0.1 ppm to 1%, precision  $\pm 2\%$  of reading). The gas flow rates were regulated with mass-flow controllers (MFC, Brooks Instruments model SLA5850S) while water was injected with a liquid mass flow controller (range 0–60 g/h, accuracy  $\pm 1\%$  of full scale). In case of water injection, the outlet gas from the membrane reactor (inner side) flowed through a bubbler and a desiccant column to condense and remove excess steam in order to protect the gas analyzer. As the bubbler induced a pressure increase ( $\sim 60 \text{ mbar}$ ) in the membrane tube, a second bubbler was placed at the cavity outlet (reduction side) to equilibrate the pressure. The reactor was heated by opening progressively the shutter system placed between the heliostat and the parabolic dish, to allow a slow and controlled heating of the membrane. When the target temperature was reached, the shutter was adjusted to maintain a constant temperature. The temperature was monitored thanks to B-type thermocouples (T1, T2, T3, and T4) along with a solar-blind pyrometer pointing on the membrane upper surface. T1 was placed below the membrane tube, in contact with its outer wall, T2 was in contact with the cavity outer wall, T3 was placed at the cavity bottom, and T4 was inserted into the membrane tube below the alumina pipe (Figure 3). The pressure in the reactor was measured by three pressure transmitters placed at both gas inlets and in the cavity. The pressures inside the membrane tube and within the cavity were maintained equal with a mechanical pressure regulator (metal diaphragm) to avoid undesired gas exchange between the inner side of the membrane and the

cavity in case the membrane was not completely densified (or not fully impermeable to molecular gas species in the course of the solar experiments, due to cracks formation).

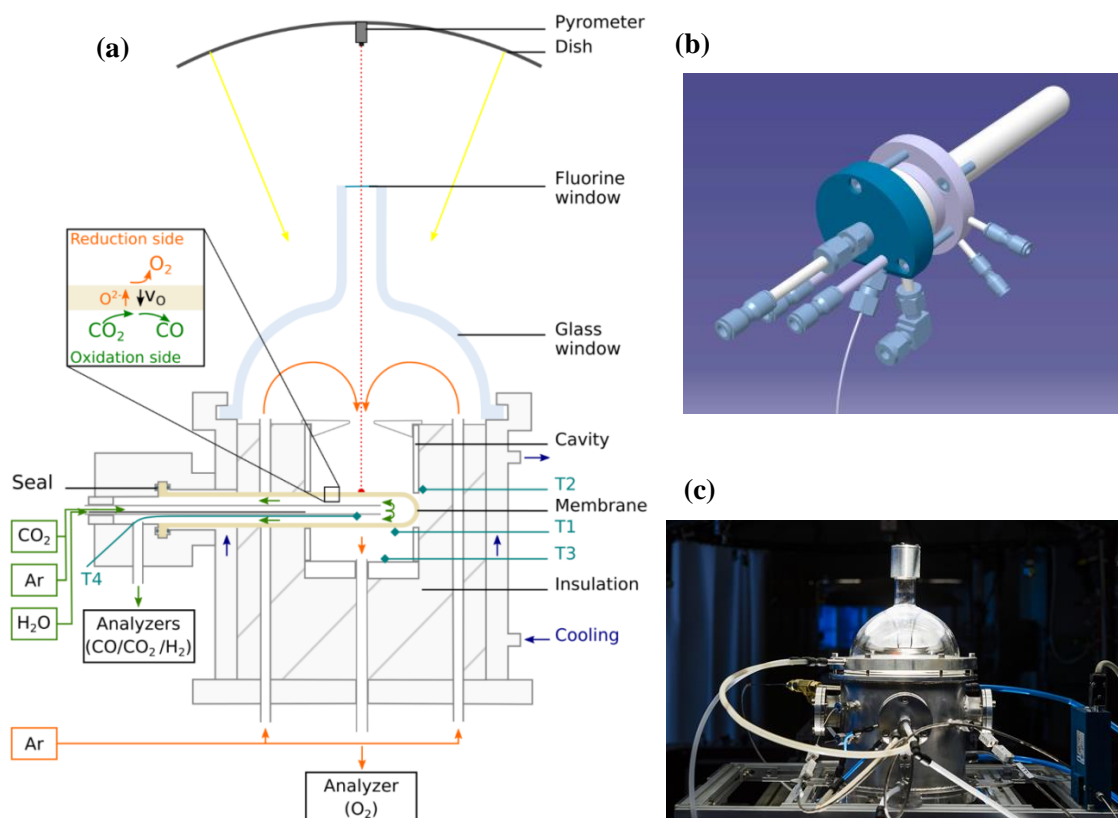


Figure 3: (a) Schematic representation of the SUNFUEL solar reactor with dead-end tubular oxygen-conducting redox membrane configuration, (b) tubular membrane before insertion within the cavity, (c) solar reactor operated at the focus of a parabolic dish solar furnace

### 3. Results and discussion

#### 3.1. Solar membrane reactor performance and stability

This experimental study addresses the solar thermochemical splitting of  $\text{CO}_2$  (or  $\text{H}_2\text{O}$ ) in the ceria membrane reactor for *in-situ* separation of  $\text{CO}$  (or  $\text{H}_2$ ) and  $\text{O}_2$  via lattice oxygen transfer and generation of synthetic solar fuels. In order to assess the performance of the isothermal solar membrane reactor, different operating conditions were studied. The impact of these conditions on both  $\text{O}_2$  and fuel production rates was investigated. Table 1 summarizes all the operating conditions along with the measured gas production rates for the three reactive membranes. In total,  $782 \mu\text{mol}/\text{cm}^2$ ,  $602 \mu\text{mol}/\text{cm}^2$  and  $1987 \mu\text{mol}/\text{cm}^2$  of  $\text{CO}$  were produced with UC, PCC1 and PCC2 membranes after a total operation time under solar radiation of 7.5 h, 5 h and 8.5 h, respectively.

Figure 4 presents the steady-state O<sub>2</sub> and CO production rates. During the heating ramp, the O<sub>2</sub> production rate increased rapidly (starting at 800°C, measured at T4) up to a peak and decreased to reach an almost stable O<sub>2</sub> production rate. When the temperature decreased, the O<sub>2</sub> production dropped quickly because the reduction was thermodynamically unfavorable. On the contrary, during reactor cooling, the oxidation was thermodynamically favored, thus the CO production rate increased. The total O<sub>2</sub>, CO and H<sub>2</sub> amounts produced by the UC, PCC1 and PCC2 membranes were calculated by the integration of associated production rates. The data are reported in Table 2.

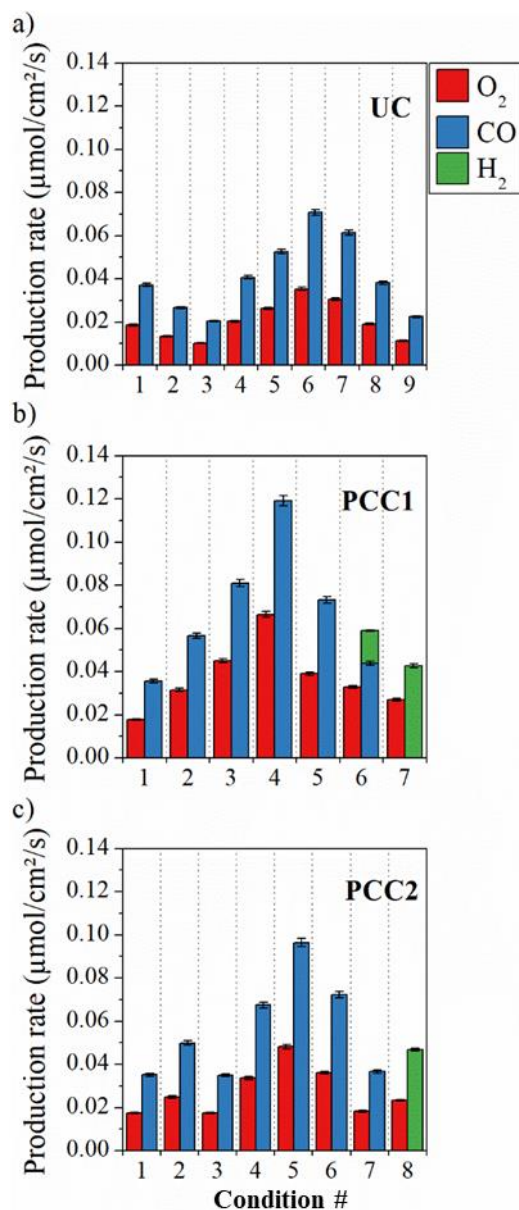


Figure 4: O<sub>2</sub>, CO and H<sub>2</sub> production rates at steady state for all the investigated operating conditions (Table 1) for a) UC, b) PCC1, and c) PCC2 membranes.

Table 1: Summary of the operating reactor parameters used for each membrane, along with the gas production rates achieved at steady-state.  $Q_{red,tot}$  and  $Q_{ox,tot}$  represent the total gas flow rate on the reduction and oxidation side, respectively (values given at normal conditions, 0°C, 1 atm)

Condition #	Membrane	Temperature (°C)	$Q_{red,tot}$ (L/min)	Oxidant gas	$Q_{ox,tot}$ (L/min)	Oxidant molar fraction	O <sub>2</sub> production rate (±2%) (μmol/cm <sup>2</sup> /s)	CO production rate (±2%) (μmol/cm <sup>2</sup> /s)	H <sub>2</sub> production rate (±2%) (μmol/cm <sup>2</sup> /s)
1	UC	1496	1.0	CO <sub>2</sub>	0.4	1.00	0.019	0.037	-
2	UC	1497	1.0	CO <sub>2</sub>	0.4	0.50	0.013	0.027	-
3	UC	1496	1.0	CO <sub>2</sub>	0.4	0.25	0.010	0.020	-
4	UC	1501	1.0	CO <sub>2</sub>	0.4	1.00	0.020	0.041	-
5	UC	1499	1.0	CO <sub>2</sub>	1.0	1.00	0.026	0.053	-
6	UC	1548	1.0	CO <sub>2</sub>	1.0	1.00	0.035	0.071	-
7	UC	1547	1.0	CO <sub>2</sub>	0.4	1.00	0.031	0.061	-
8	UC	1499	1.0	CO <sub>2</sub>	0.4	1.00	0.019	0.038	-
9	UC	1448	1.0	CO <sub>2</sub>	0.4	1.00	0.011	0.023	-
1	PCC1	1499	1.0	CO <sub>2</sub>	0.4	0.50	0.018	0.036	-
2	PCC1	1508	1.0	CO <sub>2</sub>	0.4	1.00	0.032	0.063	-
3	PCC1	1501	1.0	CO <sub>2</sub>	1.0	1.00	0.045	0.090	-
4	PCC1	1553	1.0	CO <sub>2</sub>	1.0	1.00	0.066	0.133	-
5	PCC1	1548	1.0	CO <sub>2</sub>	0.4	1.00	0.039	0.078	-
6	PCC1	1548	1.0	CO <sub>2</sub> /H <sub>2</sub> O	0.4	0.5 CO <sub>2</sub> /0.5 H <sub>2</sub> O	0.033	0.049	0.017
7	PCC1	1550	1.0	H <sub>2</sub> O	0.4	0.50	0.027	-	0.054
1	PCC2	1499	1.0	CO <sub>2</sub>	0.4	0.50	0.018	0.035	-
2	PCC2	1499	1.0	CO <sub>2</sub>	0.4	1.00	0.025	0.050	-
3	PCC2	1499	1.0	CO <sub>2</sub>	0.4	0.50	0.017	0.035	-
4	PCC2	1501	1.0	CO <sub>2</sub>	1.0	1.00	0.034	0.067	-
5	PCC2	1548	1.0	CO <sub>2</sub>	1.0	1.00	0.048	0.096	-
6	PCC2	1547	1.0	CO <sub>2</sub>	0.4	1.00	0.036	0.072	-
7	PCC2	1548	1.0	CO <sub>2</sub>	0.4	0.50	0.018	0.037	-
8	PCC2	1545	1.0	H <sub>2</sub> O	0.4	0.50	0.023	-	0.047

Table 2:  $O_2$ , CO and  $H_2$  amounts produced by each investigated membrane

Membrane	$O_2$ amount produced	CO (and $H_2$ ) amount
	(mL)	produced (mL)
UC	291.2	453.8
PCC1	257.6	302.4 (10.1)
PCC2	689.9	1153.6 (9.2)

The continuous membrane-driven solar process for fuel production eliminates the need for the temperature swing used in two-step cycles. In the solar membrane-driven isothermal process, the gas flow production rate evolved until reaching steady-state values, meaning that the oxygen transfer from the oxidation to the reduction side was equilibrated. Figure 5 shows the transient evolution of both  $O_2$  and CO production rates during the heating ramp and after temperature stabilization at 1550°C (T4 inside the membrane) for a  $CO_2$  flow rate  $Q_{ox,tot}=1$  L/min and a  $CO_2$  molar fraction  $x_{CO_2}=1.00$ . Both  $O_2$  and CO productions were already stabilized at 1500°C, with similar  $Q_{ox,tot}$  and  $x_{CO_2}$  values. After temperature stabilization, the difference between T1 and T4 was small ( $< 20^\circ C$ ), revealing a small radial temperature gradient in the membrane. Furthermore, the difference between T1 and  $T_{pyrometer}$  was also small. Although the cavity is similar to a black-body, an uncertainty of measurement remains for the temperature measured by the pyrometer due to the unknown membrane emissivity (an emissivity value of 1 was considered). The  $O_2$  and CO production rates evolved during the transient period before reaching steady-state values. The  $O_2$  production rose with temperature increase and the  $O_2$  production peak occurred when the target temperature was reached. After the  $O_2$  peak production, the  $O_2$  production rate decreased until reaching a stable value ( $0.048 \mu mol/s/cm^2$ ). For each fixed operating condition, when the membrane reached non-stoichiometry equilibrium in its thickness, the oxygen production was only attributed to the oxygen diffusivity through the membrane, which determined the oxygen flux for the considered temperature and oxygen partial pressure gradient. The time required to reach equilibrium likely depends on the membrane thickness and microstructure. Regarding the CO production rate, it started to decrease when the temperature increased due to thermodynamic limitation. Then, as further oxygen vacancies were created in the membrane bulk, the CO production increased up to  $0.096 \mu mol/cm^2/s$  (while  $O_2$  decreased) and reached equilibrium values. During a change in operating parameters, the  $O_2$  and CO production rates evolved from a transient period towards steady-state stabilization at a ratio  $O_2:CO$  of 1:2. Once the steady-state established, the  $O_2$  and CO production rates remained constant.

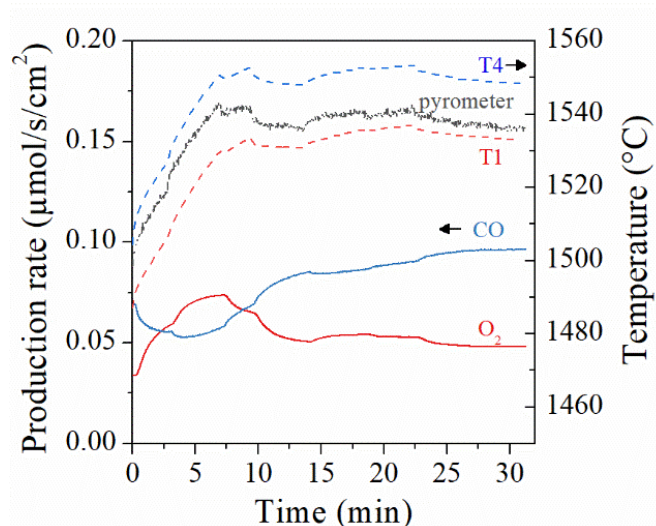


Figure 5: Evolution of the O<sub>2</sub> and CO production rates along with temperature, with  $Q_{ox,tot}=1.0$  L/min and  $x_{CO_2}=1.00$ , for the PCC2 membrane (condition #5)

An essential outcome for the membrane-driven solar process is a stable fuel production rate over time. The O<sub>2</sub> and CO production rates in steady-state under similar conditions have been measured at different period of time after the beginning of the experiment. The results confirmed that both O<sub>2</sub> and CO production rates were repeatable and stable for three similar conditions at different testing times (Figure 6), with values in the range 0.019-0.020 μmol/cm<sup>2</sup>/s and 0.037-0.041 μmol/cm<sup>2</sup>/s, respectively. Thus, the ceria membrane is clearly able to provide a stable CO production rate, with a mean value 0.039 μmol/cm<sup>2</sup>/s at 1500°C and a standard deviation of 0.002.

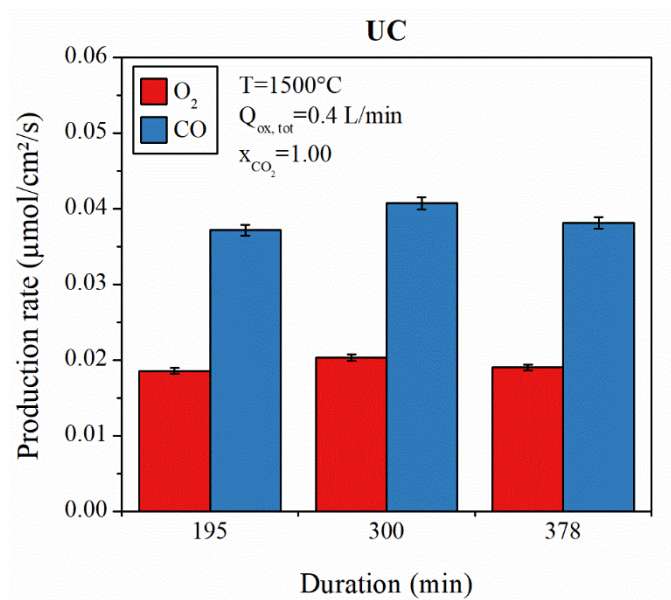


Figure 6: Evolution of O<sub>2</sub> and CO production rates as a function of the elapsed time since the experiment started, for UC ceria membrane (conditions #1, 4, and 8)

## 3.2. Influence of the operating parameters on fuel production rates

### 3.2.1. Temperature

Temperature is a key parameter in the thermochemical production of solar fuels from redox materials. As predicted by thermodynamics [29,30], the temperature influences the reduction extent of reactive materials. Thus, it was relevant to study the influence of temperature on the production rate of the reactive membranes. Figure 7.a presents the evolution of O<sub>2</sub> and CO production rates at steady state for different operating temperatures measured inside the membrane (T4). A temperature step was performed at 1400°C, but no significant CO production was observed. The temperature was then further increased until observing a start of CO production above 1400°C. For a T4 temperature of 1500°C, the temperature measured by T2 is lower than 1400°C. As T2 thermocouple is in contact with the outside cavity wall, this means that the temperature in the insulation layer is also below 1400°C. Thus, the membrane surface situated outside of the reactor cavity in the insulation layer cannot react. Hence, the reactive surface of the membrane corresponds to the surface in the cavity. As expected, it appears that increasing the temperature leads to an increase of the production rates, because it results in an increase of the reduction extent of the reactive material as well as a faster oxygen ionic conduction. Indeed, oxygen diffusivity through the membrane material requires lattice defects, specifically oxygen vacancies [26,31], and the non-stoichiometry ( $\delta$ ) depends on both the temperature and the oxygen partial pressure [29]. Thus, increasing the temperature enhances the non-stoichiometry extent achieved by the reactive oxide, which in turn promotes the CO<sub>2</sub> splitting capability. Although temperature increase cannot directly promote the CO<sub>2</sub> splitting step according to thermodynamics, results show that it still favors CO production by enhancing the oxygen transfer driving force, associated with oxygen vacancies gradient. Thus, O<sub>2</sub> and CO production rates in the redox membrane process were enhanced by a temperature rise, due to improved oxygen mobility. At 1547°C, the O<sub>2</sub> and CO production rates reached maximum values of 0.031  $\mu\text{mol}/\text{cm}^2/\text{s}$  and 0.061  $\mu\text{mol}/\text{cm}^2/\text{s}$ , respectively, and the CO<sub>2</sub> conversion extent reached 0.5 mol%. Nevertheless, the maximum operating temperature is limited by the stability of the reactive material due to fastened ageing, strong thermal gradients along the membrane axis and possible risk of sublimation [32,33]. The apparent activation energy of the reaction was determined by plotting the logarithm of the average production rate versus reverse temperatures (Figure 7.b). The activation energy for the UC membrane was  $\sim 262$  kJ/mol, while it was only  $\sim 114$  kJ/mol and  $\sim 199$  kJ/mol for PCC1 and PCC2 membranes, respectively. The lower activation energy values for PCC1 and PCC2 membranes confirm the beneficial effect of the coatings in boosting the oxygen transfer rate through the membrane. The coating on PCC2 support is less uniform than on PCC1 and the layer is thinner. Thus, the effect of the coating is more significant for the PCC1 membrane, which explains the lower activation energy value for this membrane. Consistently, the activation energy value for PCC2 lies between those for PCC1 and UC membranes.

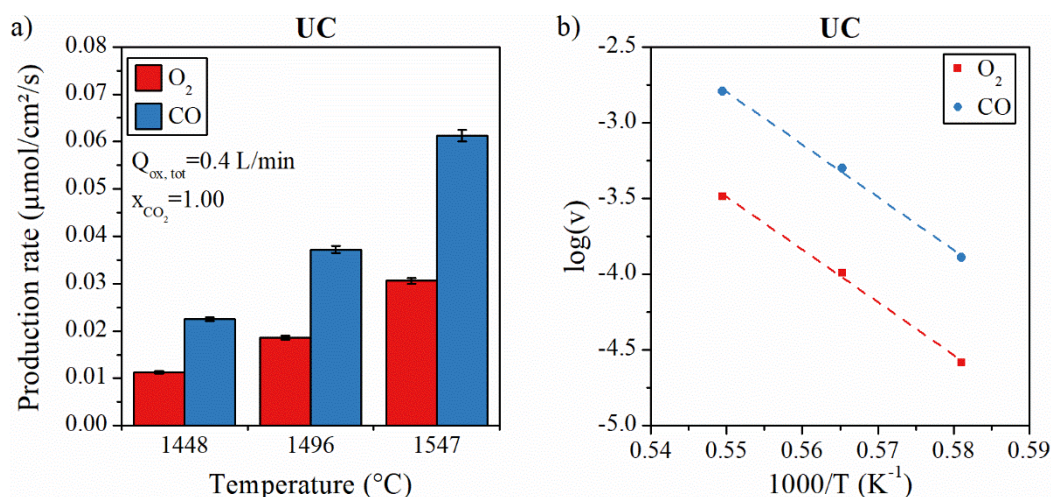


Figure 7: Influence of the reaction temperature on UC membrane performance: a) Steady state production rates for three reaction temperatures ( $T_4=1448^{\circ}\text{C}$ ,  $1496^{\circ}\text{C}$  and  $1547^{\circ}\text{C}$ , corresponding to conditions #9, 1 and 7, respectively) with a total gas flow rate of  $0.4 \text{ L/min}$  on the oxidation side and a  $\text{CO}_2$  molar fraction of  $1.00$ , and b) logarithm plot of  $\text{O}_2$  and  $\text{CO}$  production rates ( $v$ ) versus reverse temperatures ( $Q_{\text{ox,tot}}=0.4 \text{ L/min}$ ,  $x_{\text{CO}_2}=1.00$ )

### 3.2.2. Oxidant gas flow rate on the oxidation (inner) side of the membrane

In two-step thermochemical cycles, the importance of the total gas flow rate during the oxidation step was pointed out [34,35]. In the present work, the influence of the oxidant gas flow rate on the inner side ( $Q_{\text{ox,tot}}$ ) of the UC membrane was evaluated (Figure 8). Increasing  $Q_{\text{ox,tot}}$  from  $0.4 \text{ L/min}$  to  $1.0 \text{ L/min}$  improved the steady-state  $\text{O}_2$  and  $\text{CO}$  production rates from  $0.019 \mu\text{mol}/\text{cm}^2/\text{s}$  to  $0.026 \mu\text{mol}/\text{cm}^2/\text{s}$  and from  $0.038 \mu\text{mol}/\text{cm}^2/\text{s}$  to  $0.052 \mu\text{mol}/\text{cm}^2/\text{s}$ , respectively. Furthermore, the  $\text{CO}:\text{CO}_2$  ratio decreased from  $0.52\%$  to  $0.33\%$  when  $Q_{\text{ox,tot}}$  was increased, thus favoring the thermodynamic driving force toward  $\text{CO}$  production. Moreover, an increase of the total gas flow rate on the oxidation side improves mass transfer and promotes the access of the oxidant gas to the reactive surface, which favors the oxidation reaction (surface-controlled reaction), thus improving the fuel production rate. Meanwhile, dilution of gas products is enhanced and their continuous removal from the reaction sites shifts the equilibrium towards  $\text{CO}$  production. However, the increase of  $Q_{\text{ox,tot}}$  led to a decrease of the  $\text{CO}_2$  conversion extent ( $0.5\%$  at  $Q_{\text{ox,tot}}=0.4 \text{ L/min}$  versus  $0.3\%$  at  $Q_{\text{ox,tot}}=1 \text{ L/min}$ ). The  $\text{CO}_2$  conversion extent tends to follow the same behavior as the  $\text{CO}:\text{CO}_2$  ratio. In fact, the latter corresponds to the  $\text{CO}$  production rate divided by the  $\text{CO}_2$  flow rate at the reactor exit, while the  $\text{CO}_2$  conversion extent corresponds to the ratio  $(\text{CO production rate}) / (\text{CO}_2 \text{ flow rate injected})$ . The  $\text{CO}_2$  flow rate at the reactor exit is very similar to the injected  $\text{CO}_2$  flow rate, since only a small fraction of the  $\text{CO}_2$  is consumed, making the  $\text{CO}:\text{CO}_2$  ratio and the  $\text{CO}_2$  conversion extent very close. Thus, decreasing the  $\text{CO}:\text{CO}_2$  ratio to favor the oxidation reaction is achieved at the expense of a lower  $\text{CO}_2$  conversion extent. Therefore, increasing the total gas flow rate on the oxidation (inner) side of the membrane has beneficial impact on both  $\text{CO}$  and associated  $\text{O}_2$  production rates, in spite of a negative effect on the  $\text{CO}_2$  conversion extent. Similar trends were clearly observed for both PCC1 and PCC2 membranes regarding the effect of gas flow rates (Table 1). For instance (case of PCC1 membrane),

the increase of CO<sub>2</sub> flow-rate (from 0.4 L/min to 1.0 L/min) enhanced the CO production rate (from 0.063 to 0.090 μmol/cm<sup>2</sup>/s at 1500°C and from 0.078 to 0.133 μmol/cm<sup>2</sup>/s at 1550°C).

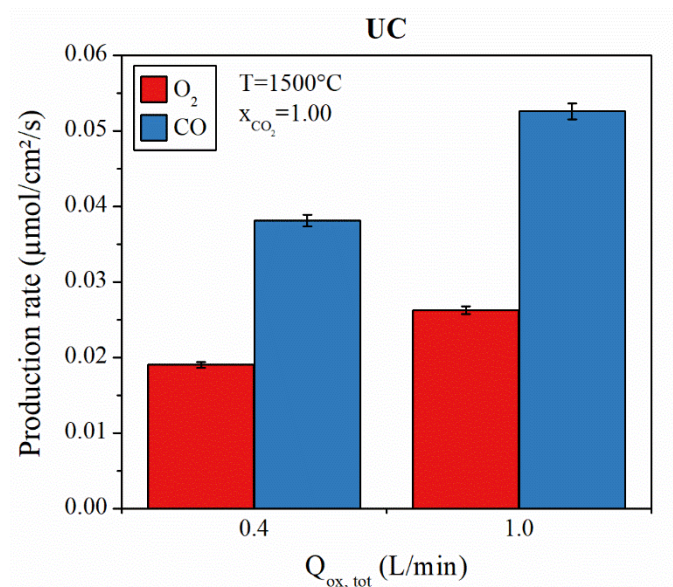


Figure 8: O<sub>2</sub> and CO production rates with total flow rates of 0.4 L/min and 1.0 L/min on the oxidation side, at 1500°C and with a CO<sub>2</sub> molar fraction of 1.00, for UC membrane (conditions #8 and 5, respectively)

### 3.2.3. Oxidant molar fraction

The CO<sub>2</sub> oxidant molar fraction was highlighted as another key parameter impacting CO production rate in two-step thermochemical cycles [34–36]. The influence of CO<sub>2</sub> molar fraction on both O<sub>2</sub> and CO production rates at steady-state was investigated, as presented in Figure 9. The CO<sub>2</sub> molar fraction was varied by adjusting the CO<sub>2</sub> and Ar inlet gas flow rates, while the total gas flow rate was maintained constant (at 0.4 L/min). Increasing the CO<sub>2</sub> molar fraction from 0.25 to 1.00 induced a rise of the O<sub>2</sub> production rate (from 0.010 μmol/cm<sup>2</sup>/s to 0.019 μmol/cm<sup>2</sup>/s) as well as the CO production rate (from 0.020 μmol/cm<sup>2</sup>/s to 0.037 μmol/cm<sup>2</sup>/s). The low value of CO:CO<sub>2</sub> ratio (0.32%) obtained with  $x_{CO_2}=1$  in comparison with 0.73% with  $x_{CO_2}=0.25$  could explain the higher membrane oxidation since the oxidation reaction is thermodynamically favored by a low CO:CO<sub>2</sub> ratio. Thus, the O<sub>2</sub> and CO production rates are enhanced by increasing the CO<sub>2</sub> oxidant molar fraction because membrane oxidation on the inner side is favored.

The evolution of O<sub>2</sub> and CO production rates in transient conditions due to the variation of  $x_{CO_2}$  is shown in Figure 10. When the CO<sub>2</sub> molar fraction is modified, the oxygen flux through the membrane is no longer at equilibrium, and the O<sub>2</sub> and CO production rates evolve toward new steady-state values. Figure 10 presents the O<sub>2</sub> and CO production rates at 1500°C (T4) with  $Q_{ox,tot}=0.4$  L/min and  $x_{CO_2}=1.00$ . The O<sub>2</sub> and CO production rates were previously stabilized with  $x_{CO_2}=0.50$  at similar temperature and  $Q_{ox,tot}$  values. When the CO<sub>2</sub> molar fraction is increased from 0.50 to 1.00, the membrane surface is instantaneously re-oxidized, leading to a drastic increase of the CO production

rate. Then, the CO production rate decreases smoothly until a stable value, higher than the value previously achieved with  $x_{\text{CO}_2}=0.50$ . In the meantime, the  $\text{O}_2$  production rate increases slowly to a stable value (half the CO production rate, denoting equilibrium is achieved) due to enhanced oxygen diffusivity.

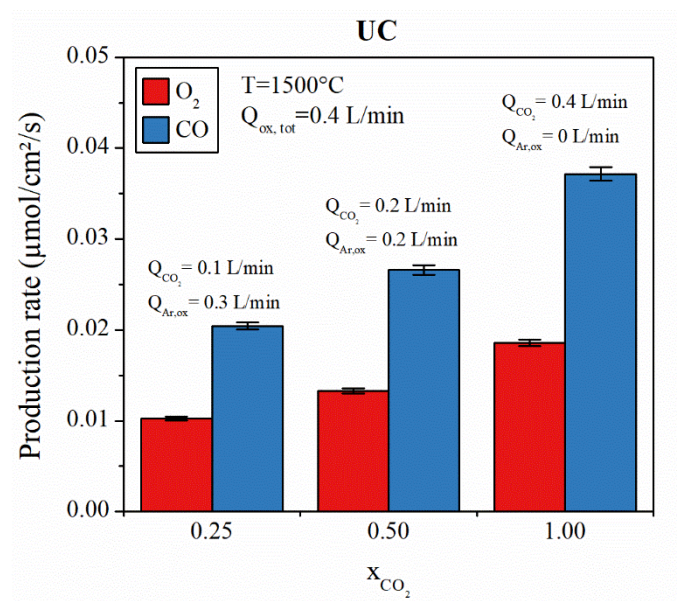


Figure 9:  $\text{O}_2$  and  $\text{CO}$  production rates in steady state conditions obtained with different  $\text{CO}_2$  molar fractions (0.25, 0.50 and 1.00, corresponding to conditions #3, 2 and 1, respectively) for UC membrane

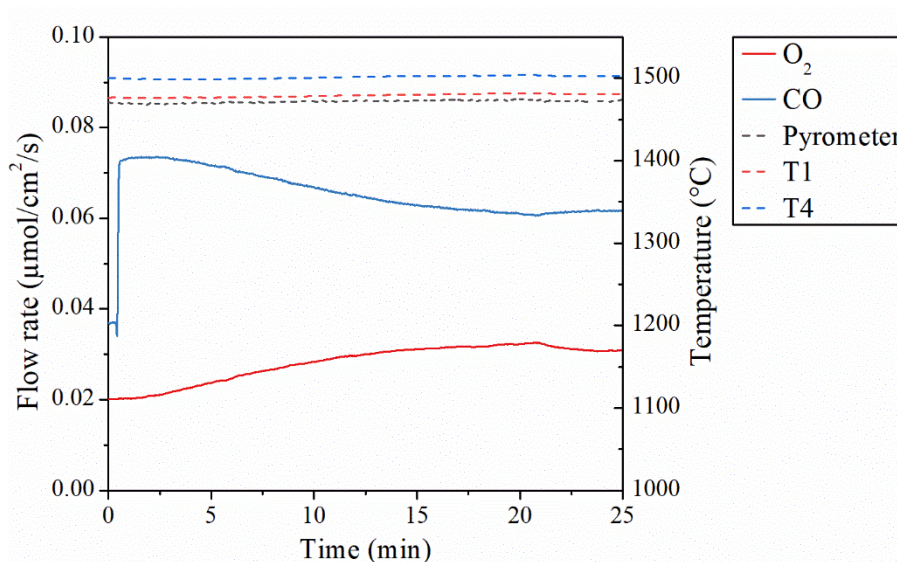


Figure 10: Evolution of  $\text{O}_2$  and  $\text{CO}$  flow rates at  $1500^\circ\text{C}$  with  $Q_{\text{ox,tot}}=0.4$  L/min after modification of the  $\text{CO}_2$  molar fraction from 0.50 to 1.00, for PCC1 membrane

### 3.2.4. Type of oxidant gas

Water and  $\text{CO}_2$  are used as oxidant gases to produce  $\text{H}_2$ ,  $\text{CO}$ , or syngas. These oxidant gases behave differently as a function of temperature due to the different thermodynamic equilibrium constants.

Actually, the dissociation temperature of H<sub>2</sub>O is higher than the CO<sub>2</sub> one, as experimentally evidenced in this study with the isothermal membrane reactor. The influence of the oxidant gas on fuel production was investigated with four oxidant gas compositions, as depicted in Figure 11. It should be noted that the water molar concentration could not be fixed at a value of 1.00 due to the necessity of using a carrier gas. With an equimolar mixture of CO<sub>2</sub> and H<sub>2</sub>O, the CO production rate (0.049 μmol/cm<sup>2</sup>/s) was higher than the H<sub>2</sub> production rate (0.017 μmol/cm<sup>2</sup>/s), due to a more favorable CO<sub>2</sub> dissociation reaction. This fits our previous results with ceria-based foams, showing that H<sub>2</sub>O is less favorable than CO<sub>2</sub> as oxidant gas [36]. Such a test demonstrates the feasibility of co-feeding both CO<sub>2</sub> and H<sub>2</sub>O, while highlighting the relative favorability of CO<sub>2</sub> thermolysis when the two co-thermolysis reactions occur simultaneously. Shortly after the water injection with 50% H<sub>2</sub>O in Ar, the reactive membrane was cracked. This event could potentially result from the occurrence of cold points created by water condensation and inducing sharp temperature gradients in the membrane material. For this reason, reaching steady-state H<sub>2</sub> production was not possible in this case. Unexpectedly, the measured H<sub>2</sub> production rate (0.054 μmol/cm<sup>2</sup>/s) with 50% H<sub>2</sub>O/Ar mixture was higher than the CO production rate (0.036 μmol/cm<sup>2</sup>/s) obtained with 50% CO<sub>2</sub>/Ar mixture. This result could however be attributed to the membrane rupture during water injection, impeding the establishment of a completed steady-state H<sub>2</sub> production rate. Thus, CO<sub>2</sub> splitting appears to be more propitious than H<sub>2</sub>O splitting as it does not induce any condensation issue and its dissociation is more favorable. However, CO production requires additional energy to separate CO from unreacted CO<sub>2</sub> while H<sub>2</sub> can be very easily purified by steam condensation.

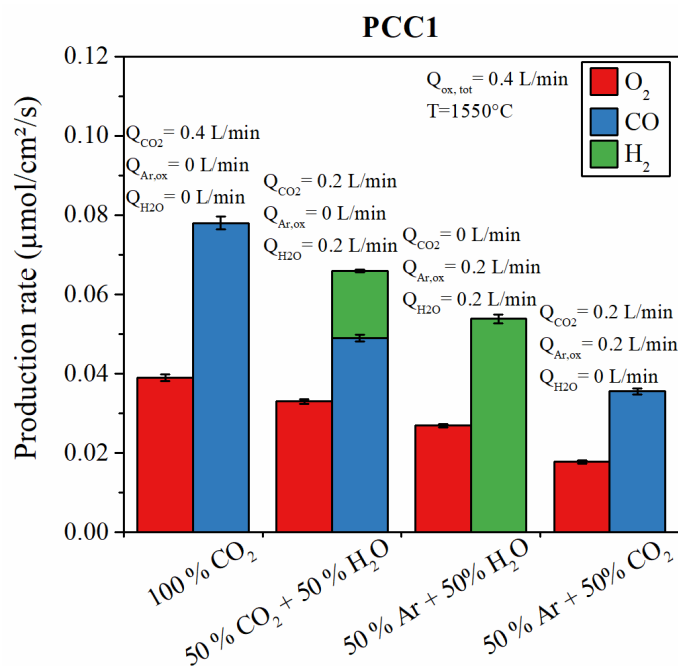


Figure 11: Comparison of O<sub>2</sub> and CO production rates with different compositions of oxidant gas, for PCC1 membrane (conditions #5, 6, 7 and 1)

### 3.2.5. Impact of reactive perovskite coatings

Dual phase perovskite-ceria composite materials (powders and foams) were previously highlighted for their enhanced thermochemical performance in comparison with pristine ceria [35,37]. In the present work, the thermochemical performances of perovskite-coated ceria membranes were compared with those of a pristine ceria membrane. The inner ceria membrane surface was coated with LSMMg layer whose fine microstructure was able to increase the available surface area for the oxidation reaction. The outer membrane surface was coated with CSM in order to favor the reduction extent of the ceria material and thus enhance the oxygen concentration gradient across the membrane thickness. Two coated membranes were tested, differing mainly by the length of the tube inserted in the cavity (shorter for PCC1). Figure 12 compares the O<sub>2</sub> and CO production rates at steady state for uncoated and coated ceria membranes. Enhanced O<sub>2</sub> and CO production rates were clearly obtained for both coated membranes, although limited improvement was measured for the longer PCC2 one. This result was attributed to a less uniform coating on the PCC2 membrane (Figure 2), highlighting the key-role of a continuous and uniform reactive perovskite coating on the ceria membrane. At 1550°C with  $Q_{\text{ox,tot}}=1.0$  L/min and  $x_{\text{CO}_2}=1.00$ , higher O<sub>2</sub> and CO production rates were obtained for both PCC1 (0.066  $\mu\text{mol}/\text{cm}^2/\text{s}$  and 0.133  $\mu\text{mol}/\text{cm}^2/\text{s}$ , respectively) and PCC2 membranes (0.048  $\mu\text{mol}/\text{cm}^2/\text{s}$  and 0.096  $\mu\text{mol}/\text{cm}^2/\text{s}$ , respectively), in comparison with the UC membrane (0.035  $\mu\text{mol}/\text{cm}^2/\text{s}$  and 0.071  $\mu\text{mol}/\text{cm}^2/\text{s}$ , respectively). Moreover, whatever the operating conditions, the CO production rates were enhanced in the range 27-72% and 18-36% for PCC1 and PCC2 membranes respectively, in comparison with the UC membrane. This clearly demonstrates the beneficial role of the perovskite coatings. The improvement of the production capacity with the reactive thin coatings can be attributed to the higher reduction of the membrane material, enhancing the oxygen mobility. Addition of an easily reducible phase (CSM [38,39]) on the external membrane surface promotes oxygen extraction, while the redox active phase (LSMMg [28]) on its inner surface promotes CO<sub>2</sub> dissociation. Therefore, appropriate perovskite coatings appear as an interesting lever to improve the continuous solar fuel production with ceria membranes.

While this study relates to direct thermolysis of CO<sub>2</sub> or H<sub>2</sub>O, most of previous works [17-22] used methane on the reduction side to promote oxygen extraction from the membrane (via partial oxidation of methane), which in turn drastically increased the obtained fuel production rate. Thus, the performance of processes involving methane reforming cannot compare with the current study on direct thermolysis. In the study of Tou et al. [26] using a pure ceria membrane reactor for direct CO<sub>2</sub> thermolysis, a maximum CO production rate of 0.024  $\mu\text{mol}/\text{cm}^2/\text{s}$  was reached with the following operating conditions:  $p_{\text{O}_2}=10^{-6}$  bar,  $T=1600^\circ\text{C}$ ,  $Q_{\text{ox,tot}}=0.2$  L/min and  $x_{\text{CO}_2}=1.00$ . In the present work, at 1500°C with a total flow rate of 0.4 L/min on the oxidation side and a CO<sub>2</sub> molar fraction of 1.00, the achieved CO production rate at steady state was 0.038  $\mu\text{mol}/\text{cm}^2/\text{s}$ , 0.063  $\mu\text{mol}/\text{cm}^2/\text{s}$  and 0.050  $\mu\text{mol}/\text{cm}^2/\text{s}$  with UC, PCC1 and PCC2 membranes, respectively. Despite a lower operating temperature, these values are much higher than those measured by Tou et al. [7,26]. These attractive

performances could be explained by more favorable operating conditions in the present work, in particular a higher total gas flow rate on the oxidation side, favoring the membrane material re-oxidation, as previously highlighted in section 3.2.2 (another important reason is likely the presence of gas leakage in [7], as ascertained by gas-tightness tests showing the noticeable effect of Ar flow rate on CO<sub>2</sub> dilution on the sweep side and Ar retrodiffusion on the CO<sub>2</sub> feed side). Therefore, an optimization of the operating parameters is a key aspect to achieve high fuel production. For all the investigated membranes, the maximum CO production rates (0.071 μmol/cm<sup>2</sup>/s, 0.133 μmol/cm<sup>2</sup>/s, and 0.096 μmol/cm<sup>2</sup>/s for UC, PCC1, and PCC2, respectively) were achieved for the following optimized operating conditions: T=1550°C, Q<sub>ox,tot</sub>=1 L/min and x<sub>CO<sub>2</sub></sub>=1.00 (Figure 12). Other parameters are likely to impact the gas production rates, such as the Ar flow rate on the reduction side (influencing both mass transfer of gaseous oxygen and oxygen partial pressure). Decreasing the oxygen partial pressure on the reduction side via dilution or with either mechanical or thermochemical pumping [40] should further promote the oxygen transfer through the membrane.

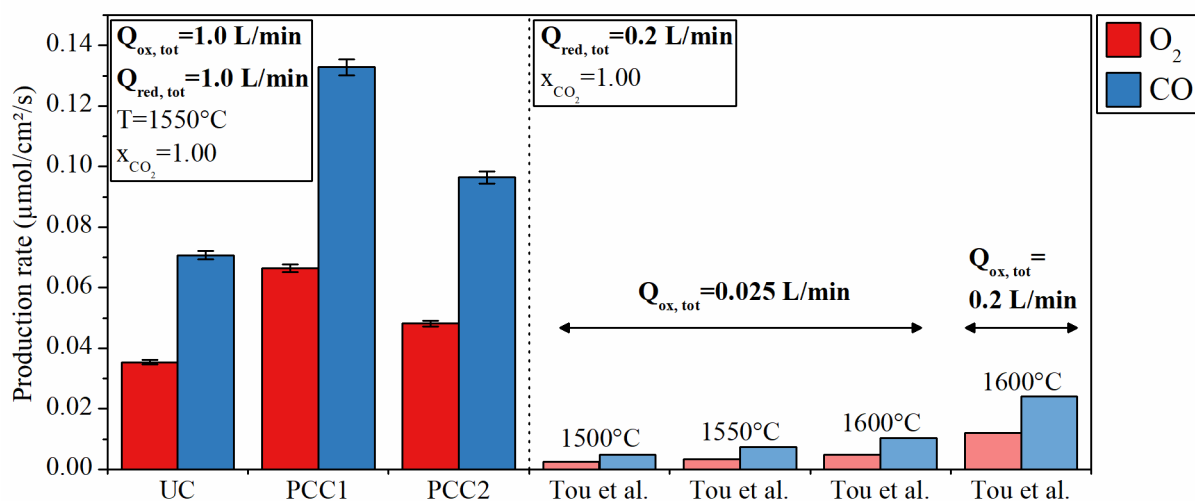


Figure 12: Comparison of O<sub>2</sub> and CO production rates obtained in this work for pristine ceria (UC: condition #6) and for coated-ceria membranes (PCC1: condition #4 and PCC2: condition #5), and by Tou et al. [26]

### 3.3. Microstructural analysis of the reactive membranes and thermal stability

The membrane surface microstructure is an important characteristic as the oxidation reaction is surface-controlled. The microstructure of the ceria membrane surface and its perovskite layers were investigated by SEM (Figure 13 and 14). Figure 13 confirms that the CSM and LSMMg coatings are not perfectly uniform on the ceria surface, and the layer thickness varies typically in the range 10-25 μm for CSM and 0.5-3 μm for LSMMg. The fresh UC membrane features grain sizes in the range 3-12 μm, while the grain sizes of the fresh CSM and LSMMg coatings are in the range 10-25 μm and 1-5 μm, respectively (Figure 14). The CSM coating (reduction side) thus offers large grain sizes, whereas the LSMMg coating (oxidation side) provides smaller grain sizes in comparison with the

uncoated UC membrane. Lowering the grain sizes on the oxidation side with the LSMMg coating should enhance the reactive membrane oxidation by favoring surface exchanges. However, as shown in Figure 14, strong sintering was evidenced after membrane utilization in the solar reactor. Ceria grain sizes increased in the range 8-30  $\mu\text{m}$ , while those of LSMMg and CSM coatings grew in the range 5-40  $\mu\text{m}$ . This sintering may be attributed to long term testing at a temperature similar to (or slightly above) the initial membrane sintering temperature in air. This sintering/grain growth could be mitigated by sintering the coated membranes at higher temperature, clearly above the reactor operating temperature. The coatings were sintered at 1500°C in this work, but it can be anticipated that a temperature of ~1600°C would be more suitable for efficient stabilization of the membrane microstructure.

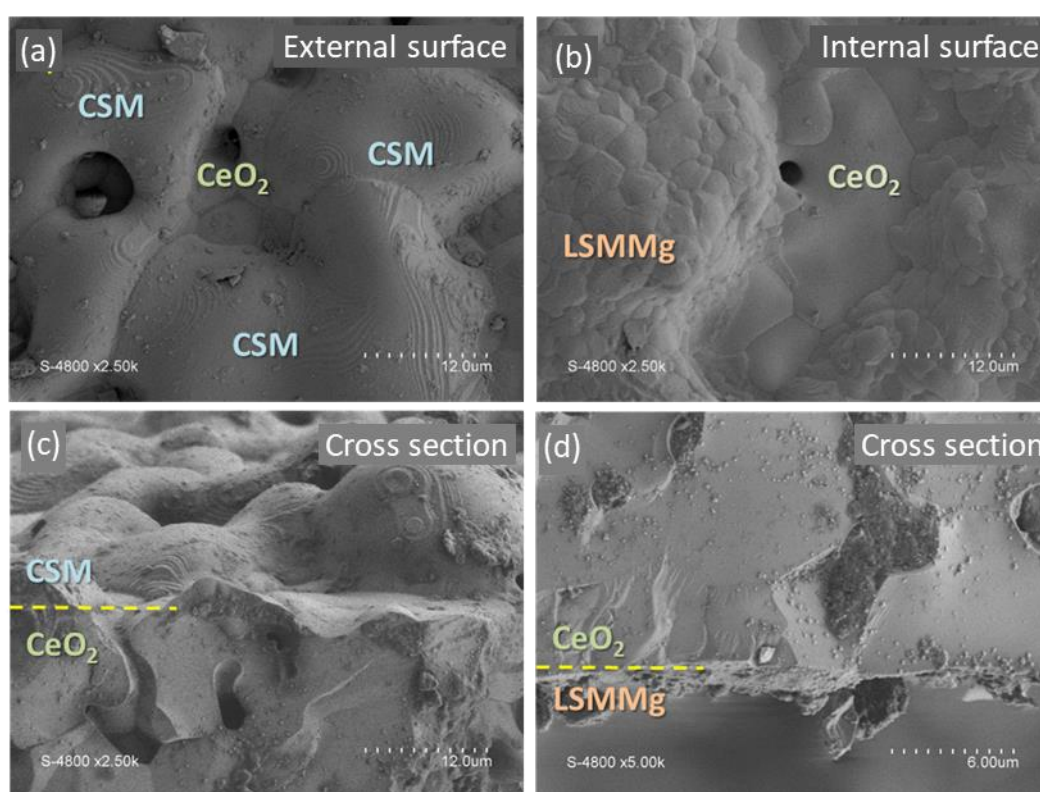


Figure 13: SEM images of the perovskite coatings on external and internal surfaces of the  $\text{CeO}_2$  support after thermal treatment in air (1500°C, 8h): (a,b) surface and (c,d) cross section of CSM and LSMMg coatings

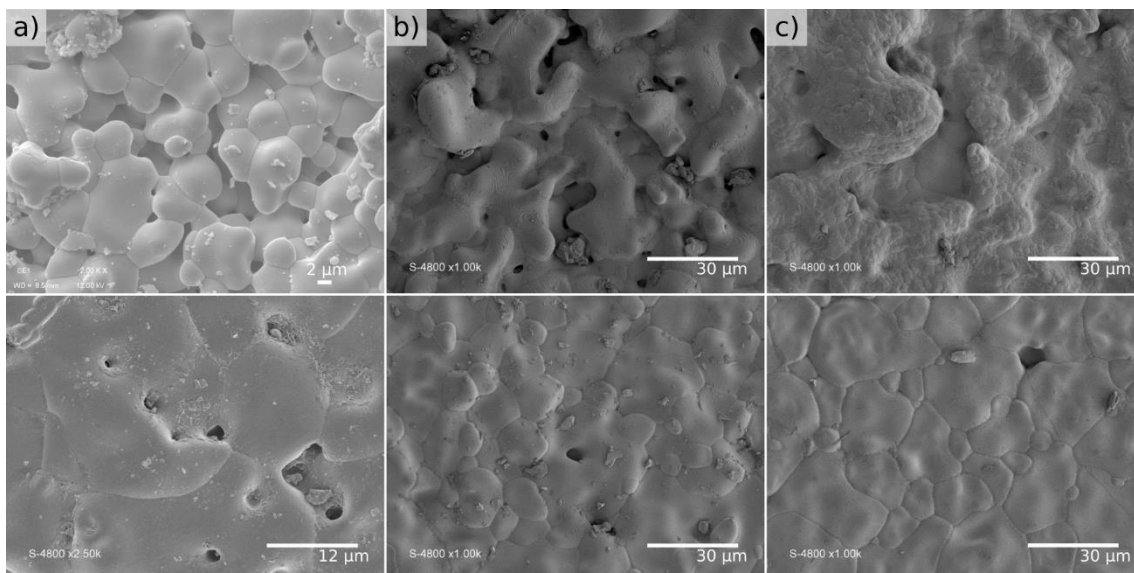


Figure 14: SEM images of the surface of: a) pristine UC ceria membrane, b) CSM coating and c) LSMMg coating before (top) and after (below) their utilization in the solar reactor

In view of future large-scale implementation, the reactive membranes should be able to undergo long term on-sun operation as well as heating/cooling steps inherent with daily-sun cycling. The thermo-mechanical stability of the reactive membrane was evaluated. During this first lab-scale study, the UC, PCC1 and PCC2 membranes were tested during 7.5 h, 5 h and 8.5 h of on-sun operation respectively. The membranes were brittle after solar tests and the weakened areas corresponded to zones submitted to high thermal gradients: located either between the cavity and the insulation, or close to the water-cooling parts of the reactor. The appearance of cracks is the result of the low resistance of ceria to thermal gradients and stresses, due to its low thermal conductivity and high thermal dilatation. In addition, the different oxidizing/reducing gas atmospheres applied on both sides and the difference in oxygen vacancies concentration creates crystallographic constraints (e.g. lattice expansion) that may also weaken the membranes. It should be underlined that the PCC2 membrane underwent a cooling and re-heating test (over two consecutive days) without any failure, thus highlighting the possibility to preserve its mechanical integrity with “slow” cooling ramp ( $\sim 13^{\circ}\text{C}/\text{min}$ ) and using only  $\text{CO}_2$  as oxidant gas. An alteration of the reactive coating on the PCC2 membrane was observed, in comparison with the original one, although no significant decline of the thermochemical performance was evidenced. The stable  $\text{O}_2$  and  $\text{CO}$  production rates obtained under similar conditions at different processing durations (as illustrated in Figure 6) confirm that the thermochemical performance of membranes is not greatly affected by thermal stresses and sintering. Since isothermal membrane operation does not induce any thermal cycling (with associated thermal shocks), the main issue is the resistance to thermal gradients along membrane length. Further improvement of the membrane thermo-mechanical resistance to thermal stress should be pursued to strengthen membrane durability and process sustainability.

### 3.4. Discussion about possible membrane process improvements

Different membrane configurations in the SUNFUEL reactor were investigated with a detailed parametric study for several membrane structures (pure ceria or sandwich-like perovskite-coated ceria) in the form of dead-end tubes inserted inside the reactor cavity and directly irradiated. The pristine ceria tubular supports, specially developed for the SUNFUEL reactor, were tested as a reference. Continuous and isothermal redox splitting of CO<sub>2</sub> (and H<sub>2</sub>O) using an oxygen conducting membrane was demonstrated in a solar reactor using real concentrated solar flux. The reactive membranes underwent full day lasting few hours of on-sun operation, highlighting their resistance to high temperatures (over 1500°C) maintained in dwell. However, temperature gradients existing along the membrane length (from the fixing side on the support to the zone located in the irradiated cavity) caused strong thermal stresses and weaknesses. After their utilization, the membranes turned out to be fragile and required specific attention during heating and cooling steps. For solar process implementation, the membrane should withstand both long on-sun operation duration and heating/cooling cycles due to daily sun-cycling. In this respect, future research should focus on the improvement of the thermomechanical resistance of membranes, especially by minimizing the impact of thermal gradients and maintaining low heating/cooling rates (typically below 5°C/min). In addition, for future reactor design, cold point should be avoided to limit steam condensation which may be responsible for membrane failure.

Regarding membrane composition, perovskite-coated ceria membranes were found to outperform pure ceria membrane, pointing out the interest to boost the oxygen transfer rate by developing dual-phase membranes consisting of thin films coated on ceria support. Membranes made entirely of perovskites could also be investigated to offer higher oxygen conductivity at lower temperatures (below 1400°C). In addition, perfectly dense thin layers coated on a porous support could provide an ideal microstructure with high available specific surface area on the oxidation side, able to further enhance the thermochemical performance. In this work, densified perovskite layers were deposited on both sides of ceria tubular supports and investigated in the solar reactor. Single coatings on each side of the support (not tested due to the lack of available supports) would need to be studied to distinguish their individual effects. Moreover, the isothermal continuous solar fuel production could be further enhanced by lowering the oxygen partial pressure on the membrane reduction side. A first option would be to increase the inert gas flow, sweeping the released oxygen from the membrane surface, which induces energy penalty for inert gas recycling. The oxygen partial pressure could also be decreased by mechanical pumping. In this case, the reactive membrane should be perfectly sealed and completely dense to avoid any transfer of molecular gas species from the oxidation to the reduction side due to the pressure gradient. An alternative to mechanical pumping is thermochemical pumping for consuming only the released oxygen [40]. For this option, a different reactor design including thermochemical pumping should be used.

The characteristics of a two-step process and a continuous membrane process can be compared. In two-step thermochemical cycles, temperature and pressure swings impose severe thermo-mechanical stress to the material as well as energy losses. Moreover, the generated fuel and O<sub>2</sub> are temporally separated in different alternating steps and thus are not produced continuously. In contrast, the membrane process occurs at high temperature but in isothermal conditions (no thermal shocks in steady state), while the fuel and O<sub>2</sub> are spatially separated during the reactions, enabling continuous production. In both isothermal thermolysis and two-step processes, the products are produced separately, thus avoiding unwanted recombination.

A direct comparison of the amount of fuel produced by the isothermal membrane and the two-step redox process is not straightforward. Indeed, the amount of fuel produced with two-step cycles depends on the mass of reactive material loaded in the reactor, whereas it is linked to the membrane active surface for the single-step membrane process. A simple attempt to compare the performance of both processes can be based on the solar-to-fuel conversion efficiency. Due to the discontinuous fuel production in a two-step thermochemical cycle, the global solar-to-fuel efficiency should be calculated for the whole cycle, defined as the ratio of the calorific value of the fuel to the total solar energy input during the cycle [34–36]. Thus, increasing the amount of fuel produced (linked to the amount of reacting redox material in the reactor) and reducing the cycling duration (linked to the reaction kinetics) is of prime importance to increase the global efficiency. For the single-step membrane process, the solar-to-fuel conversion efficiency can be determined according to equation (3):

$$\eta_{single\ step} = \frac{\dot{n}_{fuel} HHV_{fuel}}{P_{solar}} \quad (3)$$

where  $\dot{n}_{fuel}$  represents the fuel production rate at steady state,  $HHV_{fuel}$  the high heating value of the fuel and  $P_{solar}$  the solar power input at steady state. The PCC1 membrane produced 0.133  $\mu\text{mol}/\text{cm}^2/\text{s}$  of CO (at 1550°C with  $x_{\text{CO}_2}=1$  and  $Q_{\text{ox, tot}}=1$  L/min) and the associated solar-to-fuel conversion efficiency was below 1%, similar to the global efficiencies of two-step cycles at lab-scale. At this reactor scale (1.5 kW), the amounts of reactive material and available membrane surface strongly impact the solar-to-fuel conversion efficiency. However, no attempt was done to optimize the solar-to-fuel conversion efficiency in the reactor. The membrane reactive surface could be directly increased by using an array of tubular membranes placed inside the reactor cavity. Decreasing heat losses and using a heat recuperation system to recover the sensible heat of outlet gas streams for preheating inlet gas streams might also be suitable options. Therefore, further optimizations are still required to extrapolate the process at larger scale. The two-step process (with temperature swing) globally favors fuel production due to high  $\Delta\delta$  ( $\delta_{\text{red}}-\delta_{\text{ox}}$ , with  $\delta$  the oxygen under-stoichiometry in  $\text{CeO}_{2-\delta}$ ), but heat recovery systems are required and reaction kinetics need to be optimized to reduce cycling times. In contrast, the direct isothermal thermolysis via redox membrane (with oxygen partial pressure gradient)

spatially separates the gas products while alleviating heat losses and thermal shocks, and achieves continuous and simultaneous production of O<sub>2</sub> and H<sub>2</sub>/CO, but high  $\Delta\delta$  and membrane stability need to be searched.

#### 4. Conclusion

In this study, solar fuels were produced isothermally (at 1450-1550°C) with a solar-driven single step thermolysis process using reactive tubular membranes. In total, 1.91 L of CO and 0.02 L of H<sub>2</sub> were produced, highlighting the ability of the SUNFUEL reactor to provide solar fuels in a continuous redox membrane process with *in-situ* separation of reaction products. All the tested reactive membranes were able to produce continuously solar fuels, during up to 8.5 h. The reuse of membrane during different operating days also revealed possible, provided that the cooling step down to room temperature was slow enough and controlled. The influence of the main operating parameters was investigated. A temperature increase improved the CO production rate as it enhanced the oxygen mobility through the membrane due to the creation of oxygen vacancies. Increasing the total gas flow rate or the oxidant molar fraction on the membrane oxidation side, favored CO production as the membrane re-oxidation was boosted. Consequently, the oxygen permeation flux and the fuel production rate were favored at high temperature, with high gas flow rate and high oxidant molar fraction on the oxidation side. The fuel production rate could be further enhanced by lowering the oxygen partial pressure on the reduction side using either mechanical pumping or thermochemical oxygen pumping. Unprecedented fuel production rate (up to 0.071  $\mu\text{mol}/\text{cm}^2/\text{s}$  at 1550°C) was achieved with the uncoated ceria membrane integrated in the solar reactor heated by real concentrated solar radiation, thus outperforming (by a factor of about x10) the maximum values previously reported for the direct thermolysis process (i.e., without any reducer). Such attractive performance could possibly result from more favorable oxidation conditions (higher inlet gas flow rates).

Regarding the oxidant gas influence, CO<sub>2</sub> dissociation was more favorable than H<sub>2</sub>O dissociation. Furthermore, H<sub>2</sub>O may cause thermal stress due to undesired steam condensation in the cold part of the membrane, which could potentially lead to membrane breakage. Without any doubt, H<sub>2</sub> production in the solar membrane reactor will deserve further investigation as it offers capital interest for industry. Moreover, an innovative composite ceria-based membrane, coated with perovskite materials, was implemented in the reactor. The perovskite coatings were found to improve both O<sub>2</sub> and CO production rates as they boosted the creation of oxygen vacancies in the membrane materials. Dual CSM and LSMMg thin coatings on both sides of the ceria membrane appeared as promising to enhance the thermochemical performance of the pristine ceria membrane. A maximum CO production rate over 0.13  $\mu\text{mol}/\text{cm}^2/\text{s}$  was reached with the coated membrane (at 1550°C with a CO<sub>2</sub> molar fraction of 100% and a total flow rate on the oxidation side of 1 L/min). These results outperformed

the maximum rates reported for a pure ceria membrane reactor. Under the used conditions, all the tested membranes turned to be embrittled after few hours of utilization, mainly because of thermal stress and predominantly upon steam injection. This underlines the necessity to further enhance the thermo-mechanical resistance of the reactive membranes, in order to allow for longer time utilization with both CO<sub>2</sub> and H<sub>2</sub>O, with day/night cycling. In future study, the ability of the reactive membranes to produce solar fuels over long duration during successive days should be demonstrated.

## Acknowledgments

This work was funded by the French National Agency for Research (ANR, SUNFUEL project, contract N°ANR-16-CE06-0010). The authors thank R. Garcia (PROMES) for solar reactor design, and ALSYS-CTI (B. Cartoixa and V. Bollee) for supplying the pristine tubular ceria supports.

## References

- [1] S. Abanades, P. Charvin, G. Flamant, P. Neveu, Screening of water-splitting thermochemical cycles potentially attractive for hydrogen production by concentrated solar energy, *Energy*. 31 (2006) 2805–2822. <https://doi.org/10.1016/j.energy.2005.11.002>.
- [2] C. Agrafiotis, M. Roeb, C. Sattler, A review on solar thermal syngas production via redox pair-based water/carbon dioxide splitting thermochemical cycles, *Renew. Sustain. Energ. Rev.* 42 (2015) 254–285. <https://doi.org/10.1016/j.rser.2014.09.039>.
- [3] R. Pullar, R. Novais, A. Caetano, A. Barreiros, S. Abanades, F. Oliveira, A review of solar thermochemical CO<sub>2</sub> splitting using ceria-based ceramics with designed morphologies and microstructures, *Front. Chem.* 7 (2019) 601. <https://doi.org/10.3389/fchem.2019.00601>.
- [4] S. Abanades, Thermogravimetry Analysis of CO<sub>2</sub> and H<sub>2</sub>O Reduction from Solar Nanosized Zn Powder for Thermochemical Fuel Production, *Ind. Eng. Chem. Res.* 51 (2012) 741–750. <https://doi.org/10.1021/ie202518k>.
- [5] A. Haeussler, S. Abanades, J. Jouannaux, A. Julbe, Non-Stoichiometric Redox Active Perovskite Materials for Solar Thermochemical Fuel Production: A Review, *Catalysts*. 8 (2018) 611–631. <https://doi.org/10.3390/catal8120611>.
- [6] M.M. Nair, S. Abanades, Experimental screening of perovskite oxides as efficient redox materials for solar thermochemical CO<sub>2</sub> conversion, *Sustainable Energy Fuels*. 2 (2018) 843–854. <https://doi.org/10.1039/C7SE00516D>.
- [7] M. Tou, A Membrane Reactor for the Solar Thermolysis of CO<sub>2</sub> and H<sub>2</sub>O: A Thermodynamic and Experimental Analysis, Doctoral dissertation, ETH Zurich, 2019. <https://doi.org/10.3929/ethz-b-000332855>.
- [8] J. Sunarso, S. Baumann, J.M. Serra, W.A. Meulenber, S. Liu, Y.S. Lin, J.C. Diniz da Costa, Mixed ionic–electronic conducting (MIEC) ceramic-based membranes for oxygen separation, *J. Membr. Sci.* 320 (2008) 13–41. <https://doi.org/10.1016/j.memsci.2008.03.074>.
- [9] W. Deibert, M.E. Ivanova, S. Baumann, O. Guillon, W.A. Meulenber, Ion-conducting ceramic membrane reactors for high-temperature applications, *J. Membr. Sci.* 543 (2017) 79–97. <https://doi.org/10.1016/j.memsci.2017.08.016>.
- [10] F. Schulze-Küppers, S. Baumann, W.A. Meulenber, H.J.M. Bouwmeester, Influence of support layer resistance on oxygen fluxes through asymmetric membranes based on perovskite-type oxides SrTi<sub>1-x</sub>Fe O<sub>3-δ</sub>, *J. Membr. Sci.* 596 (2020) 117704. <https://doi.org/10.1016/j.memsci.2019.117704>.

- [11] X.-Y. Wu, A.F. Ghoniem, Mixed ionic-electronic conducting (MIEC) membranes for thermochemical reduction of CO<sub>2</sub>: A review, *Prog. Energy Combust. Sci.* 74 (2019) 1–30. <https://doi.org/10.1016/j.peccs.2019.04.003>.
- [12] E.M. Pfaff, A. Kaletsch, C. Broeckmann, Design of a Mixed Ionic/Electronic Conducting Oxygen Transport Membrane Pilot Module, *Chem. Eng. Technol.* 35 (2012) 455–463. <https://doi.org/10.1002/ceat.201100447>.
- [13] C. Abughayada, Air separation and oxygen storage properties of hexagonal rare-earth manganites., Doctoral dissertation, Northern Illinois University, 2015. <https://commons.lib.niu.edu/handle/10843/18551>.
- [14] U. Balachandran, J.T. Dusek, S.M. Sweeney, Methane to syngas via ceramic membranes, *Am. Ceram. Soc. Bull.* 74 (1995) 71–75.
- [15] R. Michalsky, D. Neuhaus, A. Steinfeld, Carbon Dioxide Reforming of Methane using an Isothermal Redox Membrane Reactor, *Energy Technol.* 3 (2015) 784–789. <https://doi.org/10.1002/ente.201500065>.
- [16] H. Jiang, L. Xing, O. Czuprat, H. Wang, S. Schirrmeyer, T. Schiestel, J. Caro, Highly effective NO decomposition by in situ removal of inhibitor oxygen using an oxygen transporting membrane, *Chem. Commun.* (2009) 6738. <https://doi.org/10.1039/b912269a>.
- [17] Z. Gong, L. Hong, Integration of air separation and partial oxidation of methane in the La<sub>0.4</sub>Ba<sub>0.6</sub>Fe<sub>0.8</sub>Zn<sub>0.2</sub>O<sub>3-δ</sub> membrane reactor, *J. Membr. Sci.* 380 (2011) 81–86. <https://doi.org/10.1016/j.memsci.2011.06.033>.
- [18] H. Jiang, H. Wang, S. Werth, T. Schiestel, J. Caro, Simultaneous Production of Hydrogen and Synthesis Gas by Combining Water Splitting with Partial Oxidation of Methane in a Hollow-Fiber Membrane Reactor, *Angew. Chem. Int. Ed.* 47 (2008) 9341–9344. <https://doi.org/10.1002/anie.200803899>.
- [19] W. Jin, C. Zhang, X. Chang, Y. Fan, W. Xing, N. Xu, Efficient Catalytic Decomposition of CO<sub>2</sub> to CO and O<sub>2</sub> over Pd/Mixed-Conducting Oxide Catalyst in an Oxygen-Permeable Membrane Reactor, *Environ. Sci. Technol.* 42 (2008) 3064–3068. <https://doi.org/10.1021/es702913f>.
- [20] K. Zhang, G. Zhang, Z. Liu, J. Zhu, N. Zhu, W. Jin, Enhanced stability of membrane reactor for thermal decomposition of CO<sub>2</sub> via porous-dense-porous triple-layer composite membrane, *J. Membr. Sci.* 471 (2014) 9–15. <https://doi.org/10.1016/j.memsci.2014.06.060>.
- [21] L. Nalbandian, A. Evdou, V. Zaspalis, La<sub>1-x</sub>Sr<sub>x</sub>M<sub>y</sub>Fe<sub>1-y</sub>O<sub>3-δ</sub> perovskites as oxygen-carrier materials for chemical-looping reforming, *Int. J. Hydrogen Energy.* 36 (2011) 6657–6670. <https://doi.org/10.1016/j.ijhydene.2011.02.146>.
- [22] L. Nalbandian, A. Evdou, V. Zaspalis, La<sub>1-x</sub>Sr<sub>x</sub>MO<sub>3</sub> (M = Mn, Fe) perovskites as materials for thermochemical hydrogen production in conventional and membrane reactors, *Int. J. Hydrogen Energy.* 34 (2009) 7162–7172. <https://doi.org/10.1016/j.ijhydene.2009.06.076>.
- [23] N. Itoh, M.A. Sanchez, W.-C. Xu, K. Haraya, M. Hongo, Application of a membrane reactor system to thermal decomposition of CO<sub>2</sub>, *J. Membr. Sci.* 77 (1993) 245–253. [https://doi.org/10.1016/0376-7388\(93\)85073-6](https://doi.org/10.1016/0376-7388(93)85073-6).
- [24] Y. Nigara, K. Watanabe, K. Kawamura, J. Mizusaki, M. Ishigame, Oxygen Permeation in ZrO<sub>2</sub> - CeO<sub>2</sub> - CaO for Application to Oxygen Separation from Thermally Decomposed H<sub>2</sub>O, *J. Electrochem. Soc.* 144 (1997) 1050–1055. <https://doi.org/10.1149/1.1837529>.
- [25] H. Naito, Hydrogen production from direct water splitting at high temperatures using a ZrO<sub>2</sub>-TiO<sub>2</sub>-Y<sub>2</sub>O<sub>3</sub> membrane, *Solid State Ionics.* 79 (1995) 366–370. [https://doi.org/10.1016/0167-2738\(95\)00089-0](https://doi.org/10.1016/0167-2738(95)00089-0).
- [26] M. Tou, R. Michalsky, A. Steinfeld, Solar-Driven Thermochemical Splitting of CO<sub>2</sub> and In Situ Separation of CO and O<sub>2</sub> across a Ceria Redox Membrane Reactor, *Joule.* 1 (2017) 146–154. <https://doi.org/10.1016/j.joule.2017.07.015>.
- [27] M. Tou, J. Jin, Y. Hao, A. Steinfeld, R. Michalsky, Solar-driven co-thermolysis of CO<sub>2</sub> and H<sub>2</sub>O and in-situ oxygen removal across a non-stoichiometric ceria membrane, *React. Chem. Eng.* (2019). <https://doi.org/10.1039/C8RE00218E>.
- [28] J. Jouannaux, A. Haeussler, M. Drobek, A. Ayrat, S. Abanades, A. Julbe, Lanthanum manganite perovskite ceramic powders for CO<sub>2</sub> splitting: Influence of Pechini synthesis parameters on sinterability and reactivity, *Ceram. Int.* 45 (2019) 15636–15648. <https://doi.org/10.1016/j.ceramint.2019.05.075>.

- [29] W.C. Chueh, S.M. Haile, A thermochemical study of ceria: exploiting an old material for new modes of energy conversion and CO<sub>2</sub> mitigation, *Phil. Trans. R. Soc. A.* 368 (2010) 3269–3294. <https://doi.org/10.1098/rsta.2010.0114>.
- [30] B. Bulfin, F. Call, M. Lange, O. Lübben, C. Sattler, R. Pitz-Paal, I.V. Shvets, Thermodynamics of CeO<sub>2</sub> Thermochemical Fuel Production, *Energ. Fuel.* 29 (2015) 1001–1009. <https://doi.org/10.1021/ef5019912>.
- [31] X. Dong, W. Jin, N. Xu, K. Li, Dense ceramic catalytic membranes and membrane reactors for energy and environmental applications, *Chem. Commun.* 47 (2011) 10886. <https://doi.org/10.1039/c1cc13001c>.
- [32] S. Abanades, G. Flamant, Thermochemical hydrogen production from a two-step solar-driven water-splitting cycle based on cerium oxides, *Sol. Energy.* 80 (2006) 1611–1623. <https://doi.org/10.1016/j.solener.2005.12.005>.
- [33] P. Furler, J. Scheffe, M. Gorbar, L. Moes, U. Vogt, A. Steinfeld, Solar Thermochemical CO<sub>2</sub> Splitting Utilizing a Reticulated Porous Ceria Redox System, *Energ. Fuel.* 26 (2012) 7051–7059. <https://doi.org/10.1021/ef3013757>.
- [34] A. Haeussler, S. Abanades, A. Julbe, J. Jouannaux, B. Cartoixa, Solar thermochemical fuel production from H<sub>2</sub>O and CO<sub>2</sub> splitting via two-step redox cycling of reticulated porous ceria structures integrated in a monolithic cavity-type reactor, *Energy.* 201 (2020) 117649. <https://doi.org/10.1016/j.energy.2020.117649>.
- [35] A. Haeussler, S. Abanades, A. Julbe, J. Jouannaux, B. Cartoixa, Two-step CO<sub>2</sub> and H<sub>2</sub>O splitting using perovskite-coated ceria foam for enhanced green fuel production in a porous volumetric solar reactor, *Journal of CO<sub>2</sub> Utilization.* 41 (2020) 101257. <https://doi.org/10.1016/j.jcou.2020.101257>.
- [36] A. Haeussler, S. Abanades, A. Julbe, J. Jouannaux, M. Drobek, A. Ayrál, B. Cartoixa, Remarkable performance of microstructured ceria foams for thermochemical splitting of H<sub>2</sub>O and CO<sub>2</sub> in a novel high-temperature solar reactor, *Chem. Eng. Res. Des.* 156 (2020) 311–323. <https://doi.org/10.1016/j.cherd.2020.02.008>.
- [37] A.H. Bork, A.J. Carrillo, Z.D. Hood, B. Yildiz, J.L.M. Rupp, Oxygen Exchange in Dual-phase La<sub>0.65</sub>Sr<sub>0.35</sub>MnO<sub>3</sub>-CeO<sub>2</sub> Composites for Solar Thermochemical Fuel Production, *ACS Appl. Mater. Interfaces.* 12 (2020) 32622–32632. <https://doi.org/10.1021/acsami.0c04276>.
- [38] B. Bulfin, J. Vieten, D.E. Starr, A. Azarpira, C. Zachäus, M. Hävecker, K. Skorupska, M. Schmücker, M. Roeb, C. Sattler, Redox chemistry of CaMnO<sub>3</sub> and Ca<sub>0.8</sub>Sr<sub>0.2</sub>MnO<sub>3</sub> oxygen storage perovskites, *J. Mater. Chem. A.* 5 (2017) 7912–7919. <https://doi.org/10.1039/C7TA00822H>.
- [39] L. André, S. Abanades, Investigation of metal oxides, mixed oxides, perovskites and alkaline earth carbonates/hydroxides as suitable candidate materials for high-temperature thermochemical energy storage using reversible solid-gas reactions, *Mater. Today Energy.* 10 (2018) 48–61. <https://doi.org/10.1016/j.mtener.2018.08.007>.
- [40] S. Brendelberger, J. Vieten, M.J. Vidyasagar, M. Roeb, C. Sattler, Demonstration of thermochemical oxygen pumping for atmosphere control in reduction reactions, *Sol. Energy.* 170 (2018) 273–279. <https://doi.org/10.1016/j.solener.2018.05.063>.